[Article] Free vibration analysis of functionally graded shells by a higher-order shear deformation theory and radial basis functions collocation, accounting for through-the-thickness deformations

Original Citation:
Neves A.M.A.; Ferreira A.J.M.; Carrera E.; Cinefra M.; Roque C.M.C.; Jorge R.M.N.; Soares C.M.M. (2013). *Free vibration analysis of functionally graded shells by a higher-order shear deformation theory and radial basis functions collocation, accounting for through-the-thickness deformations.* In: EUROPEAN JOURNAL OF MECHANICS. A, SOLIDS, vol. 37, pp. 24-34. - ISSN 0997-7538

Availability:
This version is available at : http://porto.polito.it/2497350/ since: May 2012

Publisher:
Elsevier

Published version:
DOI:10.1016/j.euromechsol.2012.05.005

Free vibration analysis of functionally graded shells by a higher-order shear deformation theory and radial basis functions collocation, accounting for through-the-thickness deformations

A. M. A. Neves [a], A. J. M. Ferreira [b], E. Carrera [c], M. Cinefra [c], C. M. C. Roque [d], R. M. N. Jorge [a], C. M. M. Soares [e]

[a] *Departamento de Engenharia Mecânica, Faculdade de Engenharia, Universidade do Porto, Rua Dr. Roberto Frias, 4200-465 Porto, Portugal*

[b] *(Corresponding author: ferreira@fe.up.pt)*
Departamento de Engenharia Mecânica, Faculdade de Engenharia, Universidade do Porto, Rua Dr. Roberto Frias, 4200-465 Porto, Portugal

[c] *Departament of Aeronautics and Aerospace Engineering, Politecnico di Torino, Corso Duca degli Abruzzi, 24, 10129 Torino, Italy*

[d] *INEGI, Faculdade de Engenharia, Universidade do Porto, Rua Dr. Roberto Frias, 4200-465 Porto, Portugal*

[e] *Instituto Superior Técnico, Av. Rovisco Pais, Lisboa, Portugal*

Abstract

This paper deals with free vibration problems of functionally graded shells. The analysis is performed by radial basis functions collocation, according to a higher-order shear deformation theory that accounts for through-the-thickness deformation.

The equations of motion and the boundary conditions are obtained by Carrera's Unified Formulation resting upon the principle of virtual work, and further interpolated by collocation with radial basis functions.

Numerical results include spherical as well as cylindrical shell panels with all edges clamped or simply supported and demonstrate the accuracy of the present approach.

Keywords: functionally graded materials; shells; free vibration.

1 Introduction

Functionally graded materials (FGM) are a class of composite materials that were first proposed by Bever and Duwez [1] in 1972. In a typical FGM shell the material properties continuously vary over the thickness direction by mixing two different materials [2]. The computational modelling of FGM is an important tool to the understanding of the structures behavior, and has been the target of intense research [2–8]. The continuous development of new structural materials leads to ever increasingly complex structural designs that require careful analysis. Although analytical techniques are very important, the use of numerical methods to solve shell mathematical models of complex structures has become essential.

The most common numerical procedure for the analysis of the shells is the finite element method [9–13]. This paper considers collocation with radial basis fuctions as a meshless technique. A radial basis function, $\phi(\|x - x_j\|)$ depends on the Euclidian distance between distinct collocation points $x_{j,j} = 1, 2, ..., N \in \mathbb{R}^n$. The unsymmetrical Kansa method [14] is employed in this work, for its good accuracy and easy implementation. The use of radial basis function for the analysis of structures and materials has been previously studied [15–29]. The authors have applied the RBF collocation to the analysis of composite beams and plates [30–32]. The combination of CUF and meshless methods has been performed in [33–36] for laminated plates, in [37,38] for laminated shells, and in [39,40] for FGM plates.

In this paper it is investigated for the first time how the Unified Formulation by Carrera [41–45,9] can be combined with radial basis functions collocation to the free vibration analysis of thin and thick FG shells, using a higher-order shear deformation theory (HSDT), allowing for through-the-thickness deformations. The effect of $\epsilon_{zz} \neq 0$ in these problems is also investigated. The quality of the present method in predicting free vibrations of thin and thick FG shells is demonstrated through numerical examples.

2 The Unified Formulation applied to shell HSDT

The Unified Formulation (UF) proposed by Carrera has been applied in several finite element analysis of beams, plates, and shells, either using the Principle of Virtual Displacements, or by using the Reissner's Mixed Variational theorem. The stiffness matrix components, the external force terms or the inertia terms can be obtained directly with this UF, irrespective of the shear deformation theory being considered. We present in the following the details of the formulation.

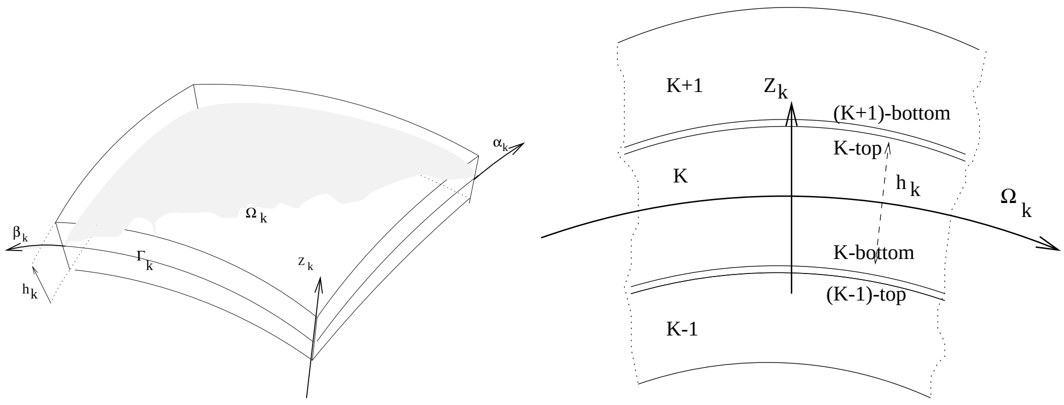

Fig. 1. Geometry and notations for a multilayered shell (doubly curved).

2.1 Shell geometry

Shells are bi-dimensional structures in which one dimension (in general the thickness in z direction) is negligible with respect to the other two in-plane dimensions. The CUF formulation applied to FGM shells considers virtual (mathematical) layers of constant thickness. The geometry and the reference system are indicated in Fig. (1).

2.2 A higher-order shear deformation theory

The present higher-order shear deformation theory involves the following expansion of displacements

$$u(\alpha,\beta,z,t) = u_0(\alpha,\beta,t) + zu_1(\alpha,\beta,t) + z^3u_3(\alpha,\beta,t) \tag{1}$$

$$v(\alpha,\beta,z,t) = v_0(\alpha,\beta,t) + zv_1(\alpha,\beta,t) + z^3v_3(\alpha,\beta,t) \tag{2}$$

$$w(\alpha,\beta,z,t) = w_0(\alpha,\beta,t) + zw_1(\alpha,\beta,t) + z^2w_2(\alpha,\beta,t) \tag{3}$$

where u, v, and w are the displacements in the $\alpha-$, $\beta-$, and $z-$ directions, respectively. u_0, u_1, u_3, v_0, v_1, v_3, w_0, w_1, and w_2 are functions to be determined. u_0, v_0 and w_0 are translations of a point at the middle-surface of the shell, and u_1, v_1, u_3, v_3 denote rotations. The consideration of higher-order terms in w allows the study of the thickness-stretching effects.

2.3 Governing equations and boundary conditions

The functionally graded shell is divided into a number (NL) of uniform thickness layers. The square of an infinitesimal linear segment in the k-th layer, the associated infinitesimal area and volume are given by:

$$
\begin{aligned}
ds_k^2 &= \; {H_\alpha^k}^2 \, d\alpha^2 \; + \; {H_\beta^k}^2 \, d\beta^2 + {H_z^k}^2 \, dz^2 \; , \\
d\Omega_k &= H_\alpha^k H_\beta^k \, d\alpha \, d\beta \; , \\
dV_k &= \; H_\alpha^k \; H_\beta^k \; H_z^k \; d\alpha \; d\beta \; dz \; ,
\end{aligned}
\tag{4}
$$

where the metric coefficients are:

$$
H_\alpha^k = A^k(1 + z/R_\alpha^k), \quad H_\beta^k = B^k(1 + z/R_\beta^k), \quad H_z^k = 1 \; . \tag{5}
$$

k denotes the k-layer of the multilayered shell; R_α^k and R_β^k are the principal radii of curvature along the coordinates α and β respectively. A^k and B^k are the coefficients of the first fundamental form of Ω_k (Γ_k is the Ω_k boundary). In this work, the attention has been restricted to shells with constant radii of curvature (cylindrical, spherical, toroidal geometries) for which $A^k = B^k = 1$.

The Principle of Virtual Displacements (PVD) for the pure-mechanical case can be expressed as:

$$
\sum_{k=1}^{NL} \int_{\Omega_k} \int_{A_k} \left\{ \delta {\epsilon_{pG}^k}^T \sigma_{pC}^k + \delta {\epsilon_{nG}^k}^T \sigma_{nC}^k \right\} d\Omega_k dz = \sum_{k=1}^{NL} \delta L_e^k \tag{6}
$$

where Ω_k and A_k are the integration domains in plane (α,β) and z direction, respectively. Here, k indicates the layer and T the transpose of a vector. G means geometrical relations and C constitutive equations and δL_e^k is the external work for the kth layer.

Stresses and strains are separated into in-plane and normal components, denoted respectively by the subscripts p and n. The mechanical strains in the kth layer can be related to the displacement field $\boldsymbol{u}^k = \{u_\alpha^k, u_\beta^k, u_z^k\}$ via the geometrical relations:

$$
\epsilon_{pG}^k = [\epsilon_{\alpha\alpha}^k, \epsilon_{\beta\beta}^k, \epsilon_{\alpha\beta}^k]^T = (\boldsymbol{D}_p^k + \boldsymbol{A}_p^k) \, \boldsymbol{u}^k \; , \; \epsilon_{nG}^k = [\epsilon_{\alpha z}^k, \epsilon_{\beta z}^k, \epsilon_{zz}^k]^T = (\boldsymbol{D}_{n\Omega}^k + \boldsymbol{D}_{nz}^k - \boldsymbol{A}_n^k) \, \boldsymbol{u}^k \tag{7}
$$

The explicit form of the introduced arrays follows:

$$
\boldsymbol{D}_p^k = \begin{bmatrix} \frac{\partial_\alpha}{H_\alpha^k} & 0 & 0 \\ 0 & \frac{\partial_\beta}{H_\beta^k} & 0 \\ \frac{\partial_\beta}{H_\beta^k} & \frac{\partial_\alpha}{H_\alpha^k} & 0 \end{bmatrix}, \quad \boldsymbol{D}_{n\Omega}^k = \begin{bmatrix} 0 & 0 & \frac{\partial_\alpha}{H_\alpha^k} \\ 0 & 0 & \frac{\partial_\beta}{H_\beta^k} \\ 0 & 0 & 0 \end{bmatrix}, \quad \boldsymbol{D}_{nz}^k = \begin{bmatrix} \partial_z & 0 & 0 \\ 0 & \partial_z & 0 \\ 0 & 0 & \partial_z \end{bmatrix}, \tag{8}
$$

$$
\boldsymbol{A}_p^k = \begin{bmatrix} 0 & 0 & \frac{1}{H_\alpha^k R_\alpha^k} \\ 0 & 0 & \frac{1}{H_\beta^k R_\beta^k} \\ 0 & 0 & 0 \end{bmatrix}, \quad \boldsymbol{A}_n^k = \begin{bmatrix} \frac{1}{H_\alpha^k R_\alpha^k} & 0 & 0 \\ 0 & \frac{1}{H_\beta^k R_\beta^k} & 0 \\ 0 & 0 & 0 \end{bmatrix}. \tag{9}
$$

The 3D constitutive equations are given as:

$$
\begin{aligned}
\sigma_{pC}^k &= \mathbf{C}_{pp}^k \; \epsilon_{pG}^k + \mathbf{C}_{pn}^k \; \epsilon_{nG}^k \\
\sigma_{nC}^k &= \mathbf{C}_{np}^k \; \epsilon_{pG}^k + \mathbf{C}_{nn}^k \; \epsilon_{nG}^k
\end{aligned} \tag{10}
$$

In the case of functionally graded materials, the matrices $\mathbf{C}_{pp}^k$, $\mathbf{C}_{pn}^k$, $\mathbf{C}_{np}^k$, and $\mathbf{C}_{nn}^k$ are reduced to:

$$
\begin{aligned}
\mathbf{C}_{pp}^k &= \begin{bmatrix} C_{11}^k & C_{12}^k & 0 \\ C_{12}^k & C_{11}^k & 0 \\ 0 & 0 & C_{44}^k \end{bmatrix} \qquad
\mathbf{C}_{pn}^k = \begin{bmatrix} 0 & 0 & C_{12}^k \\ 0 & 0 & C_{12}^k \\ 0 & 0 & 0 \end{bmatrix} \\
\mathbf{C}_{np}^k &= \begin{bmatrix} 0 & 0 & 0 \\ 0 & 0 & 0 \\ C_{12}^k & C_{12}^k & 0 \end{bmatrix} \qquad
\mathbf{C}_{nn}^k = \begin{bmatrix} C_{44}^k & 0 & 0 \\ 0 & C_{44}^k & 0 \\ 0 & 0 & C_{33}^k \end{bmatrix}
\end{aligned} \tag{11}
$$

The computation of elastic constants C_{ij}^k for each layer, considers the following steps:

(1) computation of volume fraction of the ceramic and metal phases
(2) computation of elastic properties E^k and ν^k
(3) computation of elastic constants C_{ij}

In the present work, the volume fraction of the ceramic phase is defined according to the power-law:

$$
V_c^k = \left(0.5 + \frac{z}{h}\right)^p \tag{12}
$$

being $z \in [-h/2, h/2]$, h the thickness of the shell, and the exponent p a scalar parameter that defines gradation of material properties across the thickness direction. The volume fraction of the metal phase is given as $V_m^k = 1 - V_c^k$.

The Young's modulus, E^k, and Poisson's ratio, ν^k, are computed by the law-of-mixtures:

$$
E^k(z) = E_m V_m^k + E_c V_c^k; \qquad \nu^k(z) = \nu_m V_m^k + \nu_c V_c^k; \tag{13}
$$

Then, the computation of the elastic constants C_{ij}^k is performed, depending on the assumption of ϵ_{zz}. If $\epsilon_{zz} = 0$, then C_{ij}^k are the plane-stress reduced elastic constants:

$$C_{11}^k = \frac{E^k}{1-(\nu^k)^2}; \quad C_{12}^k = \nu^k \frac{E^k}{1-(\nu^k)^2}; \quad C_{44}^k = \frac{E^k}{2(1+\nu^k)}; \quad C_{33} = 0 \tag{14}$$

where E^k is the modulus of elasticity, ν^k is the Poisson's ratio found in previous step.

If $\epsilon_{zz} \neq 0$ (thickness-stretching), then C_{ij}^k are the three-dimensional elastic constants, given by

$$C_{11}^k = \frac{E^k(1-(\nu^k)^2)}{1-3(\nu^k)^2-2(\nu^k)^3}, \quad C_{12}^k = \frac{E^k(\nu^k+(\nu^k)^2)}{1-3(\nu^k)^2-2(\nu^k)^3} \tag{15}$$

$$C_{44}^k = \frac{E^k}{2(1+\nu^k)}, \quad C_{33}^k = \frac{E^k(1-(\nu^k)^2)}{1-3(\nu^k)^2-2(\nu^k)^3} \tag{16}$$

The three displacement components u_α, u_β and u_z (given in (1) to (3)) and their relative variations can be modelled by CUF as:

$$(u_\alpha, u_\beta, u_z) = F_\tau \ (u_{\alpha\tau}, u_{\beta\tau}, u_{z\tau}) \qquad (\delta u_\alpha, \delta u_\beta, \delta u_z) = F_s \ (\delta u_{\alpha s}, \delta u_{\beta s}, \delta u_{zs}) \tag{17}$$

where F_τ are functions of the thickness coordinate z and τ is a sum index. In the present formulation the thickness functions are

$$F_{su\alpha} = F_{su\beta} = F_{\tau u\alpha} = F_{\tau u\beta} = \begin{bmatrix} 1 & z & z^3 \end{bmatrix} \tag{18}$$

for in-plane displacements u, v and

$$F_{sw} = F_{\tau w} = \begin{bmatrix} 1 & z & z^2 \end{bmatrix} \tag{19}$$

for transverse displacement w. All the terms of the equations of motion are then obtained by integrating through the thickness direction.

Substituting the geometrical relations, the constitutive equations and the unified formulation into the variational statement PVD, for the kth layer, one obtains:

$$\sum_{k=1}^{NL}\{\int_{\Omega_k}\int_{A_k}\{((\boldsymbol{D}_p+\boldsymbol{A}_p)\delta\boldsymbol{u}^k)^T(\boldsymbol{C}_{pp}^k(\boldsymbol{D}_p+\boldsymbol{A}_p)\boldsymbol{u}^k+\boldsymbol{C}_{pn}^k(\boldsymbol{D}_{n\Omega}+\boldsymbol{D}_{nz}-\boldsymbol{A}_n)\boldsymbol{u}^k)+ \\ ((\boldsymbol{D}_{n\Omega}+\boldsymbol{D}_{nz}-\boldsymbol{A}_n)\delta\boldsymbol{u}^k)^T(\boldsymbol{C}_{np}^k(\boldsymbol{D}_p+\boldsymbol{A}_p)\boldsymbol{u}^k+\boldsymbol{C}_{nn}^k(\boldsymbol{D}_{n\Omega}+\boldsymbol{D}_{nz}-\boldsymbol{A}_n)\boldsymbol{u}^k)\}d\Omega_k dz_k\} \\ = \sum_{k=1}^{NL}\delta L_e^k \tag{20}$$

At this point, the formula of integration by parts is applied:

$$\int_{\Omega_k} \left((\mathbf{D}_\Omega)\delta\mathbf{a}^k\right)^T \mathbf{a}^k d\Omega_k = -\int_{\Omega_k} \delta\mathbf{a}^{kT} \left((\mathbf{D}_\Omega^T)\mathbf{a}^k\right) d\Omega_k + \int_{\Gamma_k} \delta\mathbf{a}^{kT} \left((\mathbf{I}_\Omega)\mathbf{a}^k\right) d\Gamma_k \tag{21}$$

where $\mathbf{I}_\Omega$ matrix is obtained applying the *Divergence theorem*:

$$\int_\Omega \frac{\partial\psi}{\partial x_i} dv = \oint_\Gamma n_i \psi ds \tag{22}$$

being n_i the components of the normal $\widehat{n}$ to the boundary along the direction i. After integration by parts and the substitution of CUF, the governing equations and boundary conditions for the shell in the mechanical case are obtained:

$$\begin{aligned}
&\sum_{k=1}^{NL}\{\int_{\Omega_k}\int_{A_k}\{\delta\boldsymbol{u}_s^{kT}[(-\boldsymbol{D}_p+\boldsymbol{A}_p)^T F_s(\boldsymbol{C}_{pp}^k(\boldsymbol{D}_p+\boldsymbol{A}_p)F_\tau\boldsymbol{u}_\tau^k+\boldsymbol{C}_{pn}^k(\boldsymbol{D}_{n\Omega}+\boldsymbol{D}_{nz}-\boldsymbol{A}_n)F_\tau\boldsymbol{u}_\tau^k)]+\\
&\delta\boldsymbol{u}_s^{kT}[(-\boldsymbol{D}_{n\Omega}+\boldsymbol{D}_{nz}-\boldsymbol{A}_n)^T F_s(\boldsymbol{C}_{np}^k(\boldsymbol{D}_p+\boldsymbol{A}_p)F_\tau\boldsymbol{u}_\tau^k+\boldsymbol{C}_{nn}^k(\boldsymbol{D}_{n\Omega}+\boldsymbol{D}_{nz}-\boldsymbol{A}_n)F_\tau\boldsymbol{u}_\tau^k)]\}d\Omega_k dz_k\}\\
&+\sum_{k=1}^{NL}\{\int_{\Gamma_k}\int_{A_k}\{\delta\boldsymbol{u}_s^{kT}[\boldsymbol{I}_p^T F_s(\boldsymbol{C}_{pp}^k(\boldsymbol{D}_p+\boldsymbol{A}_p)F_\tau\boldsymbol{u}_\tau^k+\boldsymbol{C}_{pn}^k(\boldsymbol{D}_{n\Omega}+\boldsymbol{D}_{nz}-\boldsymbol{A}_n)F_\tau\boldsymbol{u}_\tau^k)]+\\
&\delta\boldsymbol{u}_s^{kT}[\boldsymbol{I}_{np}^T F_s(\boldsymbol{C}_{np}^k(\boldsymbol{D}_p-\boldsymbol{A}_p)F_\tau\boldsymbol{u}_\tau^k+\boldsymbol{C}_{nn}^k(\boldsymbol{D}_{n\Omega}+\boldsymbol{D}_{nz}-\boldsymbol{A}_n)F_\tau\boldsymbol{u}_\tau^k)]\}d\Gamma_k dz_k\}\\
&=\sum_{k=1}^{NL}\{\int_{\Omega_k}\delta\boldsymbol{u}_s^{kT}F_s\boldsymbol{p}_u^k\}\ .
\end{aligned} \tag{23}$$

where $\mathbf{I}_p^k$ and $\mathbf{I}_{np}^k$ depend on the boundary geometry:

$$\mathbf{I}_p = \begin{bmatrix} \frac{n_\alpha}{H_\alpha} & 0 & 0 \\ 0 & \frac{n_\beta}{H_\beta} & 0 \\ \frac{n_\beta}{H_\beta} & \frac{n_\alpha}{H_\alpha} & 0 \end{bmatrix}; \mathbf{I}_{np} = \begin{bmatrix} 0 & 0 & \frac{n_\alpha}{H_\alpha} \\ 0 & 0 & \frac{n_\beta}{H_\beta} \\ 0 & 0 & 0 \end{bmatrix};. \tag{24}$$

The normal to the boundary of domain Ω is:

$$\widehat{\boldsymbol{n}} = \begin{bmatrix} n_\alpha \\ n_\beta \end{bmatrix} = \begin{bmatrix} cos(\varphi_\alpha) \\ cos(\varphi_\beta) \end{bmatrix} \tag{25}$$

where φ_α and φ_β are the angles between the normal $\widehat{n}$ and the direction α and β respectively.

The governing equations for a multi-layered shell subjected to mechanical loadings are:

$$\delta \mathbf{u}_s^{k^T} : \qquad \mathbf{K}_{uu}^{k\tau s}\, \mathbf{u}_\tau^k \;=\; \mathbf{P}_{u\tau}^k \tag{26}$$

where the fundamental nucleus $\mathbf{K}_{uu}^{k\tau s}$ is obtained as:

$$\boldsymbol{K}_{uu}^{k\tau s} = \int_{A_k} \Big[[-\boldsymbol{D}_p + \boldsymbol{A}_p]^T\, \boldsymbol{C}_{pp}^k [\boldsymbol{D}_p + \boldsymbol{A}_p] + [-\boldsymbol{D}_p + \boldsymbol{A}_p]^T\, \boldsymbol{C}_{pn}^k [\boldsymbol{D}_{n\Omega} + \boldsymbol{D}_{nz} - \boldsymbol{A}_n] + \\ [-\boldsymbol{D}_{n\Omega} + \boldsymbol{D}_{nz} - \boldsymbol{A}_n]^T\, \boldsymbol{C}_{np}^k [\boldsymbol{D}_p + \boldsymbol{A}_p] + [-\boldsymbol{D}_{n\Omega} + \boldsymbol{D}_{nz} - \boldsymbol{A}_n]^T\, \boldsymbol{C}_{nn}^k [\boldsymbol{D}_{n\Omega} + \boldsymbol{D}_{nz} - \boldsymbol{A}_n] \Big] \\ F_\tau F_s H_\alpha^k H_\beta^k \; dz \; . \tag{27}$$

and the corresponding Neumann-type boundary conditions on Γ_k are:

$$\boldsymbol{\Pi}_d^{k\tau s}\, \mathbf{u}_\tau^k \;=\; \boldsymbol{\Pi}_d^{k\tau s}\, \bar{\mathbf{u}}_\tau^k \; , \tag{28}$$

where:

$$\boldsymbol{\Pi}_d^{k\tau s} = \int_{A_k} \Big[\boldsymbol{I}_p^T\, \boldsymbol{C}_{pp}^k [\boldsymbol{D}_p + \boldsymbol{A}_p^\tau] + \boldsymbol{I}_p^T\, \boldsymbol{C}_{pn}^k [\boldsymbol{D}_{n\Omega} + \boldsymbol{D}_{nz} - \boldsymbol{A}_n^\tau] + \\ \boldsymbol{I}_{np}^T \boldsymbol{C}_{np}^k [\boldsymbol{D}_p + \boldsymbol{A}_p^\tau] + \boldsymbol{I}_{np}^T\, \boldsymbol{C}_{nn}^k [\boldsymbol{D}_{n\Omega} + \boldsymbol{D}_{nz} - \boldsymbol{A}_n^\tau] \Big] F_\tau F_s H_\alpha^k H_\beta^k \; dz \; . \tag{29}$$

and $\mathbf{P}_{u\tau}^k$ are variationally consistent loads with applied pressure.

The fundamental nucleo $\mathbf{K}_{uu}^{k\tau s}$ is reported for functionally graded doubly curved shells (radii of curvature in both α and β directions (see Fig.1)):

$$
\begin{aligned}
\left(\mathbf{K}_{uu}^{\tau sk}\right)_{11} &= -C_{11}^k J_{\beta/\alpha}^{k\tau s}\partial_\alpha^s\partial_\alpha^\tau - C_{44}^k J_{\alpha/\beta}^{k\tau s}\partial_\beta^s\partial_\beta^\tau \\
&\quad + C_{44}^k\left(J_{\alpha\beta}^{k\tau_z s_z} - \frac{1}{R_{\alpha_k}}J_\beta^{k\tau_z s} - \frac{1}{R_{\alpha_k}}J_\beta^{k\tau s_z} + \frac{1}{R_{\alpha_k}^2}J_{\beta/\alpha}^{k\tau s}\right) \\
\left(\mathbf{K}_{uu}^{\tau sk}\right)_{12} &= -C_{12}^k J^{k\tau s}\partial_\alpha^\tau\partial_\beta^s - C_{44}^k J^{k\tau s}\partial_\alpha^s\partial_\beta^\tau \\
\left(\mathbf{K}_{uu}^{\tau sk}\right)_{13} &= -C_{11}^k\frac{1}{R_{\alpha_k}}J_{\beta/\alpha}^{k\tau s}\partial_\alpha^\tau - C_{12}^k\frac{1}{R_{\beta_k}}J^{k\tau s}\partial_\alpha^\tau - C_{12}^k J_\beta^{k\tau s_z}\partial_\alpha^\tau \\
&\quad + C_{44}^k\left(J_\beta^{k\tau_z s}\partial_\alpha^s - \frac{1}{R_{\alpha_k}}J_{\beta/\alpha}^{k\tau s}\partial_\alpha^s\right) \\
\left(\mathbf{K}_{uu}^{\tau sk}\right)_{21} &= -C_{12}^k J^{k\tau s}\partial_\alpha^s\partial_\beta^\tau - C_{44}^k J^{k\tau s}\partial_\alpha^\tau\partial_\beta^s \\
\left(\mathbf{K}_{uu}^{\tau sk}\right)_{22} &= -C_{22}^k J_{\alpha/\beta}^{k\tau s}\partial_\beta^s\partial_\beta^\tau - C_{26}^k J^{k\tau s}\partial_\alpha^s\partial_\beta^\tau - C_{26}^k J^{k\tau s}\partial_\alpha^\tau\partial_\beta^s - C_{44}^k J_{\beta/\alpha}^{k\tau s}\partial_\alpha^s\partial_\alpha^\tau \\
&\quad + C_{44}^k\left(J_{\alpha\beta}^{k\tau_z s_z} - \frac{1}{R_{\beta_k}}J_\alpha^{k\tau_z s} - \frac{1}{R_{\beta_k}}J_\alpha^{k\tau s_z} + \frac{1}{R_{\beta_k}^2}J_{\alpha/\beta}^{k\tau s}\right) \\
\left(\mathbf{K}_{uu}^{\tau sk}\right)_{23} &= -C_{12}^k\frac{1}{R_{\alpha_k}}J^{k\tau s}\partial_\beta^\tau - C_{22}^k\frac{1}{R_{\beta_k}}J_{\alpha/\beta}^{k\tau s}\partial_\beta^\tau - C_{12}^k J_\alpha^{k\tau s_z}\partial_\beta^\tau \\
&\quad + C_{44}^k\left(J_\alpha^{k\tau_z s}\partial_\beta^s - \frac{1}{R_{\beta_k}}J_{\alpha/\beta}^{k\tau s}\partial_\beta^s\right) \\
\left(\mathbf{K}_{uu}^{\tau sk}\right)_{31} &= C_{11}^k\frac{1}{R_{\alpha_k}}J_{\beta/\alpha}^{k\tau s}\partial_\alpha^s + C_{12}^k\frac{1}{R_{\beta_k}}J^{k\tau s}\partial_\alpha^s + C_{12}^k J_\beta^{k\tau_z s}\partial_\alpha^s \\
&\quad - C_{44}^k\left(J_\beta^{k\tau s_z}\partial_\alpha^\tau - \frac{1}{R_{\alpha_k}}J_{\beta/\alpha}^{k\tau s}\partial_\alpha^\tau\right) \\
\left(\mathbf{K}_{uu}^{\tau sk}\right)_{32} &= C_{12}^k\frac{1}{R_{\alpha_k}}J^{k\tau s}\partial_\beta^s + C_{22}^k\frac{1}{R_{\beta_k}}J_{\alpha/\beta}^{k\tau s}\partial_\beta^s + C_{12}^k J_\alpha^{k\tau_z s}\partial_\beta^s \\
&\quad - C_{44}^k\left(J_\alpha^{k\tau s_z}\partial_\beta^\tau - \frac{1}{R_{\beta_k}}J_{\alpha/\beta}^{k\tau s}\partial_\beta^\tau\right) \\
\left(\mathbf{K}_{uu}^{\tau sk}\right)_{33} &= C_{11}^k\frac{1}{R_{\alpha_k}^2}J_{\beta/\alpha}^{k\tau s} + C_{22}^k\frac{1}{R_{\beta_k}^2}J_{\alpha/\beta}^{k\tau s} + C_{33}^k J_{\alpha\beta}^{k\tau_z s_z} \\
&\quad + 2C_{12}^k\frac{1}{R_{\alpha_k}}\frac{1}{R_{\beta_k}}J^{k\tau s} + C_{12}^k\frac{1}{R_{\alpha_k}}\left(J_\beta^{k\tau_z s} + J_\beta^{k\tau s_z}\right) + C_{12}^k\frac{1}{R_{\beta_k}}\left(J_\alpha^{k\tau_z s} + J_\alpha^{k\tau s_z}\right) \\
&\quad - C_{44}^k J_{\alpha/\beta}^{k\tau s}\partial_\beta^s\partial_\beta^\tau - C_{44}^k J_{\beta/\alpha}^{k\tau s}\partial_\alpha^s\partial_\alpha^\tau
\end{aligned}
\tag{30}
$$

where

$$
\begin{aligned}
(J^{k\tau s}, J_{\alpha}^{k\tau s}, J_{\beta}^{k\tau s}, J_{\frac{\alpha}{\beta}}^{k\tau s}, J_{\frac{\beta}{\alpha}}^{k\tau s}, J_{\alpha\beta}^{k\tau s}) &= \int_{A_k} F_\tau F_s (1, H_\alpha, H_\beta, \frac{H_\alpha}{H_\beta}, \frac{H_\beta}{H_\alpha}, H_\alpha H_\beta)\ dz \\
(J^{k\tau_z s}, J_{\alpha}^{k\tau_z s}, J_{\beta}^{k\tau_z s}, J_{\frac{\alpha}{\beta}}^{k\tau_z s}, J_{\frac{\beta}{\alpha}}^{k\tau_z s}, J_{\alpha\beta}^{k\tau_z s}) &= \int_{A_k} \frac{\partial F_\tau}{\partial z} F_s (1, H_\alpha, H_\beta, \frac{H_\alpha}{H_\beta}, \frac{H_\beta}{H_\alpha}, H_\alpha H_\beta)\ dz \\
(J^{k\tau s_z}, J_{\alpha}^{k\tau s_z}, J_{\beta}^{k\tau s_z}, J_{\frac{\alpha}{\beta}}^{k\tau s_z}, J_{\frac{\beta}{\alpha}}^{k\tau s_z}, J_{\alpha\beta}^{k\tau s_z}) &= \int_{A_k} F_\tau \frac{\partial F_s}{\partial z} (1, H_\alpha, H_\beta, \frac{H_\alpha}{H_\beta}, \frac{H_\beta}{H_\alpha}, H_\alpha H_\beta)\ dz \\
(J^{k\tau_z s_z}, J_{\alpha}^{k\tau_z s_z}, J_{\beta}^{k\tau_z s_z}, J_{\frac{\alpha}{\beta}}^{k\tau_z s_z}, J_{\frac{\beta}{\alpha}}^{k\tau_z s_z}, J_{\alpha\beta}^{k\tau_z s_z}) &= \int_{A_k} \frac{\partial F_\tau}{\partial z} \frac{\partial F_s}{\partial z} (1, H_\alpha, H_\beta, \frac{H_\alpha}{H_\beta}, \frac{H_\beta}{H_\alpha}, H_\alpha H_\beta)\ dz
\end{aligned}
\tag{31}
$$

The application of boundary conditions makes use of the fundamental nucleo $\mathbf{\Pi}_d$ in the form:

$$
\begin{aligned}
\left(\mathbf{\Pi}_{uu}^{\tau sk}\right)_{11} &= n_\alpha C_{11}^k J_{\beta/\alpha}^{k\tau s} \partial_\alpha^s + n_\beta C_{44}^k J_{\alpha/\beta}^{k\tau s} \partial_\beta^s \\
\left(\mathbf{\Pi}_{uu}^{\tau sk}\right)_{12} &= n_\alpha C_{12}^k J^{k\tau s} \partial_\beta^s + n_\beta C_{44}^k J^{k\tau s} \partial_\alpha^s \\
\left(\mathbf{\Pi}_{uu}^{\tau sk}\right)_{13} &= n_\alpha \frac{1}{R_{\alpha k}} C_{11}^k J_{\beta/\alpha}^{k\tau s} + n_\alpha \frac{1}{R_{\beta k}} C_{12}^k J^{k\tau s} + n_\alpha C_{12}^k J_{\beta}^{k\tau s_z} \\
\left(\mathbf{\Pi}_{uu}^{\tau sk}\right)_{21} &= n_\beta C_{12}^k J^{k\tau s} \partial_\alpha^s + n_\alpha C_{44}^k J^{k\tau s} \partial_\beta^s \\
\left(\mathbf{\Pi}_{uu}^{\tau sk}\right)_{22} &= n_\alpha C_{44}^k J_{\beta/\alpha}^{k\tau s} \partial_\alpha^s + n_\beta C_{22}^k J_{\alpha/\beta}^{k\tau s} \partial_\beta^s + n_\beta C_{26}^k J^{k\tau s} \partial_\alpha^s + n_\alpha C_{26}^k J^{k\tau s} \partial_\beta^s \\
\left(\mathbf{\Pi}_{uu}^{\tau sk}\right)_{23} &= n_\beta \frac{1}{R_{\alpha k}} C_{12}^k J^{k\tau s} + n_\beta \frac{1}{R_{\beta k}} C_{22}^k J_{\alpha/\beta}^{k\tau s} + n_\beta C_{12}^k J_{\alpha}^{k\tau s_z} \\
\left(\mathbf{\Pi}_{uu}^{\tau sk}\right)_{31} &= -n_\alpha \frac{1}{R_{\alpha k}} C_{44}^k J_{\beta/\alpha}^{k\tau s} + n_\alpha C_{44}^k J_{\beta}^{k\tau s_z} \\
\left(\mathbf{\Pi}_{uu}^{\tau sk}\right)_{32} &= -n_\beta \frac{1}{R_{\beta k}} C_{44}^k J_{\alpha/\beta}^{k\tau s} + n_\beta C_{44}^k J_{\alpha}^{k\tau s_z} \\
\left(\mathbf{\Pi}_{uu}^{\tau sk}\right)_{33} &= n_\alpha C_{44}^k J_{\beta/\alpha}^{k\tau s} \partial_\alpha^s + n_\beta C_{44}^k J_{\alpha/\beta}^{k\tau s} \partial_\beta^s
\end{aligned}
\tag{32}
$$

Note that all the equations written for the shell degenerate in those for the plate when $\dfrac{1}{R_{\alpha k}} = \dfrac{1}{R_{\beta k}} = 0$. In practice, the radii of curvature are set to 10^9 for analysis of plates with the present formulation.

2.5 Dynamic governing equations

The PVD for the dynamic case is expressed as:

$$\sum_{k=1}^{NL} \int_{\Omega_k} \int_{A_k} \left\{ \delta\epsilon_{pG}^{k}{}^{T} \sigma_{pC}^{k} + \delta\epsilon_{nG}^{k}{}^{T} \sigma_{nC}^{k} \right\} d\Omega_k dz = \sum_{k=1}^{NL} \int_{\Omega_k} \int_{A_k} \rho^k \delta\mathbf{u}^{kT} \ddot{\mathbf{u}}^k d\Omega_k dz + \sum_{k=1}^{NL} \delta L_e^k \tag{33}$$

where ρ^k is the mass density of the k-th layer and double dots denote acceleration.

By substituting the geometrical relations and the constitutive equations, one obtains the following governing equations:

$$\delta\mathbf{u}_s^{kT} : \qquad \mathbf{K}_{uu}^{k\tau s} \mathbf{u}_\tau^k = \mathbf{M}^{k\tau s} \ddot{\mathbf{u}}_\tau^k + \mathbf{P}_{u\tau}^k \tag{34}$$

In the case of free vibrations one has:

$$\delta\mathbf{u}_s^{kT} : \qquad \mathbf{K}_{uu}^{k\tau s} \mathbf{u}_\tau^k = \mathbf{M}^{k\tau s} \ddot{\mathbf{u}}_\tau^k \tag{35}$$

where $\mathbf{M}^{k\tau s}$ is the fundamental nucleus for the inertial term, given by

$$\begin{aligned} \mathbf{M}_{ij}^{k\tau s} &= \rho^k J_{\alpha\beta}^{k\tau s}, \quad i = j \\ \mathbf{M}_{ij}^{k\tau s} &= 0, \quad i \neq j \end{aligned} \tag{36}$$

The meaning of the integral $J_{\alpha\beta}^{k\tau s}$ has been illustrated in eq. (31). The geometrical and mechanical boundary conditions are the same of the static case.

3 The radial basis function method for free vibration problems

Consider a linear elliptic partial differential operator $\mathcal{L}$ acting in a bounded region Ω in $\mathbb{R}^n$ and another operator $\mathcal{L}_B$ acting on a boundary $\partial\Omega$. The eigenproblem looks for eigenvalues (λ) and eigenvectors ($\mathbf{u}$) that satisfy

$$\mathcal{L}\mathbf{u} + \lambda\mathbf{u} = 0 \text{ in } \Omega \tag{37}$$

$$\mathcal{L}_B\mathbf{u} = 0 \text{ on } \partial\Omega \tag{38}$$

The eigenproblem defined in (37) and (38) will be replaced by a finite-dimensional eigenvalue problem, after the radial basis approximations.

The radial basis function (ϕ) approximation of a function ($\mathbf{u}$) is given by

$$\tilde{\mathbf{u}}(\mathbf{x}) = \sum_{i=1}^{N} \alpha_i \phi \left(\|x - y_i\|_2 \right), \mathbf{x} \in \mathbb{R}^n \tag{39}$$

where $y_i, i = 1, .., N$ is a finite set of distinct points (centers) in $\mathbb{R}^n$.

Derivatives of $\tilde{\mathbf{u}}$ are computed as

$$\frac{\partial \tilde{\mathbf{u}}}{\partial x} = \sum_{j=1}^{N} \alpha_j \frac{\partial \phi_j}{\partial x} \tag{40}$$

$$\frac{\partial^2 \tilde{\mathbf{u}}}{\partial x^2} = \sum_{j=1}^{N} \alpha_j \frac{\partial^2 \phi_j}{\partial x^2}, \text{etc} \tag{41}$$

In the present collocation approach, one needs to impose essential and natural boundary conditions. Consider, for example, the condition $w = 0$, on a simply supported or clamped edge. The conditions are enforced by interpolating as

$$w = 0 \rightarrow \sum_{j=1}^{N} \alpha_j^W \phi_j = 0 \tag{42}$$

Other boundary conditions are interpolated in a similar way.

Examples of some common RBFs are

$$\begin{aligned} \text{Cubic:} \quad & \phi(r) = r^3 \\ \text{Thin plate splines:} \quad & \phi(r) = r^2 \log(r) \\ \text{Wendland functions:} \quad & \phi(r) = (1 - r)_+^m p(r) \\ \text{Gaussian:} \quad & \phi(r) = e^{-(cr)^2} \\ \text{Multiquadrics:} \quad & \phi(r) = \sqrt{c^2 + r^2} \\ \text{Inverse Multiquadrics:} \quad & \phi(r) = (c^2 + r^2)^{-1/2} \end{aligned}$$

where the Euclidian distance r is real and non-negative and c is a positive shape parameter. Considering N distinct interpolations, and knowing $u(x_j), j = 1, 2, ..., N$, one finds α_i by the solution of a $N \times N$ linear system

$$\mathbf{A}\boldsymbol{\alpha} = \mathbf{u} \tag{43}$$

where $\mathbf{A} = [\phi(\|x - y_i\|_2)]_{N \times N}$, $\boldsymbol{\alpha} = [\alpha_1, \alpha_2, ..., \alpha_N]^T$ and $\mathbf{u} = [u(x_1), u(x_2), ..., u(x_N)]^T$.

The solution of the eigenproblem by radial basis functions considers N_I nodes in the interior of the domain and N_B nodes on the boundary, witha total number of nodes $N = N_I + N_B$. The interpolation points are denoted by $x_i \in \Omega, i = 1, ..., N_I$ and $x_i \in \partial\Omega, i = N_I + 1, ..., N$. At the points in the domain, the following eigenproblem is defined

$$\sum_{i=1}^{N} \alpha_i \mathcal{L}\phi\left(\|x - y_i\|_2\right) = \lambda \tilde{\mathbf{u}}(x_j), j = 1, 2, ..., N_I \tag{44}$$

or

$$\mathcal{L}^I \boldsymbol{\alpha} = \lambda \tilde{\mathbf{u}}^I \tag{45}$$

where

$$\mathcal{L}^I = \left[\mathcal{L}\phi\left(\|x - y_i\|_2\right)\right]_{N_I \times N} \tag{46}$$

At the points on the boundary, the imposed boundary conditions are

$$\sum_{i=1}^{N} \alpha_i \mathcal{L}_B\phi\left(\|x - y_i\|_2\right) = 0, j = N_I + 1, ..., N \tag{47}$$

or

$$\mathbf{B}\boldsymbol{\alpha} = 0 \tag{48}$$

where $\mathbf{B} = \mathcal{L}_B\phi\left[\left(\|x_{N_I+1} - y_j\|_2\right)\right]_{N_B \times N}$.

Therefore, one can write a finite-dimensional eigenvalue problem and solve equations (45) and (48) as a generalized eigenvalue problem

$$\begin{bmatrix} \mathcal{L}^I \\ \mathbf{B} \end{bmatrix} \boldsymbol{\alpha} = \lambda \begin{bmatrix} \mathbf{A}^I \\ \mathbf{0} \end{bmatrix} \boldsymbol{\alpha} \tag{49}$$

where

$$\mathbf{A}^I = \phi\left[\left(\|x_{N_I} - y_j\|_2\right)\right]_{N_I \times N}$$

For free vibration problems an harmonic solution is assumed for the displacements $u_0, u_1, v_0, v_1, \cdots$

$$\begin{array}{lll} u_0 = U_0(x,y)e^{i\omega t}; & u_1 = U_1(x,y)e^{i\omega t}; & u_3 = U_3(x,y)e^{i\omega t} \\ v_0 = V_0(x,y)e^{i\omega t}; & v_1 = V_1(x,y)e^{i\omega t}; & v_3 = V_3(x,y)e^{i\omega t} \\ w_0 = W_0(x,y)e^{i\omega t}; & w_1 = W_1(x,y)e^{i\omega t}; & w_2 = W_2(x,y)e^{i\omega t} \end{array} \tag{50}$$

where ω is the frequency of natural vibration. Substituting the harmonic expansion into equations (49) in terms of the amplitudes $U_0, U_1, U_3, V_0, V_1, V_3, W_0, W_1, W_2$, one can obtain the natural frequencies and vibration modes for the plate or shell problem, by solving the eigenproblem

$$\left[\mathcal{L} - \omega^2 \mathcal{G}\right] \mathbf{X} = \mathbf{0} \tag{51}$$

where $\mathcal{L}$ collects all stiffness terms and $\mathcal{G}$ collects all terms related to the inertial terms. In (51) $\mathbf{X}$ are the modes of vibration associated with the natural frequencies defined as ω.

4 Numerical results

In this section the higher-order shear deformation theory is combined with radial basis functions collocation for the free vibration analysis of functionally graded shell panels. Examples include spherical ($R_x = R_y = R$) as well as cylindrical ($R_x = R$ and $R_y = \infty$) shell panels with all edges clamped (CCCC) or simply supported (SSSS). Particular cases of these are also considered: isotropic materials (fully ceramic, $p = 0$, and fully metal, $p = \infty$) and plates ($R_x = R_y = \infty$).

To study the effect of $\epsilon_{zz} \neq 0$ in these problems, the case $\epsilon_{zz} = 0$ is implemented by considering $w = w_0$ instead (3).

Results are compared with those from Pradyumna and Bandyopadhyay [46], who used finite elements formulation and a HSDT disregarding through-the-thickness deformations.

The following material properties are used:

silicon nitride (Si_3N_4):

$$E_c = 322.2715GPa,\ \nu_c = 0.24,\ \rho_c = 2370Kg/m^3 \tag{52}$$

stainless steel ($SUS304$):

$$E_m = 207.7877GPa,\ \nu_m = 0.31776,\ \rho_m = 8166Kg/m^3 \tag{53}$$

aluminum:

$$E_m = 70GPa,\ \nu_m = 0.3,\ \rho_m = 2707Kg/m^3 \tag{54}$$

alumina:

$$E_c = 380GPa,\ \nu_c = 0.3,\ \rho_c = 3000Kg/m^3 \tag{55}$$

The non-dimensional frequency is given as

$$\bar{w} = wa^2\sqrt{\frac{\rho_m h}{D}} \quad \text{where} \quad D = \frac{E_m h^3}{12(1-\nu_m^2)}. \tag{56}$$

In all numerical examples a Chebyshev grid is employed (see figure 2) and the

grid	13^2	17^2	19^2	21^2
1^{st}	60.3483	60.3431	60.3499	60.3479
2^{nd}	115.2450	115.2134	115.2315	115.2044
3^{rd}	115.3917	115.3665	115.3755	115.3347
4^{th}	162.1741	162.0337	162.0727	162.0860

Table 1
Initial study. Square CCCC FG cylindrical panel, Si_3N_4 and $SUS304$, $a/h = 10$, $a/R = 0.1$, $p = 0.2$.

Wendland function defined as

$$\phi(r) = (1 - c\,r)_+^8 \left(32(c\,r)^3 + 25(c\,r)^2 + 8c\,r + 1\right) \tag{57}$$

Here, the shape parameter (c) is obtained by an optimization procedure, as detailed in Ferreira and Fasshauer [47].

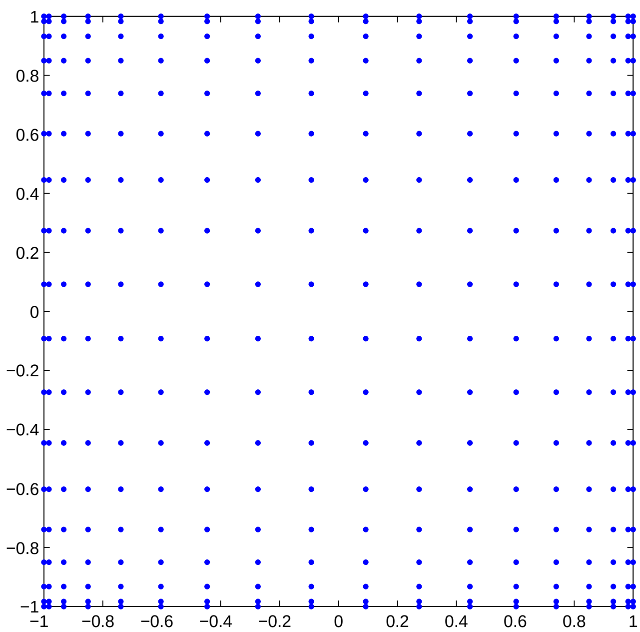

Fig. 2. A sketch of a Chebyshev grid for 17^2 points

An initial study was performed to show the convergence of the present approach and select the number of points to use in the computation of the vibration problems. Results are presented in table 1 and refer to the first four vibration modes of a clamped functionally graded cylindrical shell panel composed of silicon nitride (52) and stainless steel (53), with side-to-thickness ratio $a/h = 10$, side-to-radius ratio $a/R = 0.1$, power law exponent $p = 0.2$, and $a = b = 2$. A 17^2 grid was chosen for the following vibration problems.

mode	source	$p = 0$ (Si_3N_4)	$p = 0.2$	$p = 2$	$p = 10$	$p = \infty$ ($SUS304$)
1	ref. [46]	72.9613	60.0269	39.1457	33.3666	32.0274
	ref. [48]	74.518	57.479	40.750	35.852	32.761
	present $\epsilon_{zz} = 0$	74.2634	60.0061	40.5259	35.1663	32.6108
	present $\epsilon_{zz} \neq 0$	74.5821	60.3431	40.8262	35.4229	32.8593
2	ref. [46]	138.5552	113.8806	74.2915	63.2869	60.5546
	ref. [48]	144.663	111.717	78.817	69.075	63.314
	present $\epsilon_{zz} = 0$	141.6779	114.3788	76.9725	66.6482	61.9329
	present $\epsilon_{zz} \neq 0$	142.4281	115.2134	77.6639	67.1883	62.4886
3	ref. [46]	138.5552	114.0266	74.3868	63.3668	60.6302
	ref. [48]	145.740	112.531	79.407	69.609	63.806
	present $\epsilon_{zz} = 0$	141.8485	114.5495	77.0818	66.7332	62.0082
	present $\epsilon_{zz} \neq 0$	142.6024	115.3665	77.7541	67.2689	62.5668
4	ref. [46]	195.5366	160.6235	104.7687	89.1970	85.1788
	ref. [48]	206.992	159.855	112.457	98.386	90.370
	present $\epsilon_{zz} = 0$	199.1566	160.7355	107.9484	93.3350	86.8160
	present $\epsilon_{zz} \neq 0$	200.3158	162.0337	108.9677	94.0923	87.6341

Table 2
First 4 modes of a CCCC square FG cylindrical shell panel, Si_3N_4 and $SUS304$, $a/h = 10$, $a/R = 0.1$, for several p.

4.1 Clamped functionally graded cylindrical shell panel

The free vibration of clamped FG cylindrical shell panels is analysed.

In table 2 the first 4 vibration modes of a square clamped FG cylindrical shell panel with constituents silicon nitride (52) and stainless steel (53), side-to-thickness ratio $a/h = 10$, side-to-radius ratio $a/R = 0.1$, and several power law exponents p are presented. Results are compared with [46] and those from Yang and Shen [48], with the differential quadrature approximation and Galerkin technique, both neglecting through-the-thickness deformations.

In figure 3 the first 4 modes of a CCCC square FG cylindrical shell panel, with constituents silicon nitride and stainless steel, ratios $a/h = 10$ and $R/a = 10$, and power law exponent $p = 0.2$ are presented.

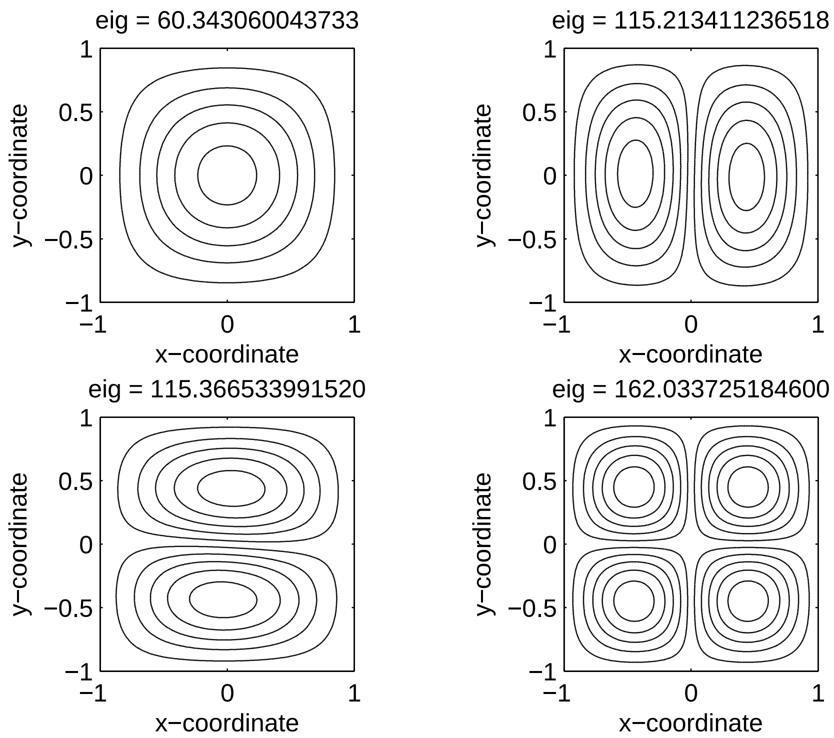

Fig. 3. First 4 modes of a CCCC square FG cylindrical shell panel, Si_3N_4 and $SUS304$, $a/h = 10$, $a/R = 0.1$, $p = 0.2$.

The fundamental frequency of square clamped FG cylindrical shell panels composed of aluminum (54) and alumina (55), with side-to-radius ratio $a/R = 0.1$, various side-to-thickness ratios a/h and power law exponents p are presented in table 3.

The results of the present approach in tables 2 and 3 compare well with references. The combination of present HSDT and the meshless technique based on collocation with radial basis function shows very good accuracy in the free vibration analysis of FG shells.

In table 4 the fundamental frequency of square clamped FG cylindrical shell panels composed of aluminum (54) and alumina (55), with side-to-thickness ratios $a/h = 10$, are presented considering various side-to-radius ratio a/R, and power law exponents p.

4.2 Simply supported functionally graded cylindrical shell panel

The free vibration of simply supported FG cylindrical shell panels is now analysed.

p	source	a/h =5	a/h =10	a/h =15	a/h =20	a/h =50	a/h =100
0	FSDT	56.5548	70.8035	75.7838	77.5654	85.4346	103.4855
	ref. [46]	58.2858	71.7395	75.0439	77.0246	84.8800	102.9227
	present $\epsilon_{zz} = 0$	59.0433	72.3272	76.4904	78.4918	85.6073	102.3351
	present $\epsilon_{zz} \neq 0$	59.7741	72.8141	76.8148	78.7342	85.7713	102.7871
0.5	FSDT	47.2468	57.7597	62.2838	63.8393	70.3199	87.1049
	ref. [46]	48.7185	58.5305	61.5835	63.1381	69.8604	86.5452
	present $\epsilon_{zz} = 0$	49.3050	59.5188	62.6780	64.2371	70.4237	85.4780
	present $\epsilon_{zz} \neq 0$	49.9508	59.9353	62.9544	64.4438	70.5664	85.9029
1	FSDT	42.0305	51.0884	55.4209	56.7991	62.8458	77.7762
	ref. [46]	43.4243	52.0173	54.7015	56.0880	62.2152	77.0774
	present $\epsilon_{zz} = 0$	43.9548	52.8776	55.6437	57.0255	62.7088	76.6386
	present $\epsilon_{zz} \neq 0$	44.5754	53.2759	55.9081	57.2226	62.8414	77.0381

Table 3
Fundamental frequencies of CCCC square FG cylindrical shell panels composed of aluminum and alumina, $R/a = 0.1$, for various a/h and p.

Table 5 presents the fundamental frequency of a square simply supported FG cylindrical shell panel with constituents aluminum (54) and alumina (55), length-to-thickness ratio $a/h = 10$, and several length-to-radius ratio a/R and several power law exponents p as well.

In figure 4 the relationships between fundamental frequency and the radius-to-length ratio R/a is visualized for various power law exponents p. It refers to the square simply supported FG cylindrical shell panel composed from aluminum (54) and alumina (55), with side-to-thickness ratio $a/h = 10$. The graphic on the left was obtained from tabulated values on table 5 and the right one is more detailed for values of p smaller or equal than 5 ($p = 0.5, 1, 2, 3, 4, 5$).

4.3 Clamped functionally graded spherical shell panel

We now study the free vibration of clamped FG spherical shell panels.

The fundamental frequency of a square clamped FG spherical shell panel with constituents aluminum (54) and alumina (55), and side-to-thickness ratio $a/h = 10$, considering various side-to-radius ratios a/R, and several power law exponents p are presented in table 6.

p	source	R/a =0.5	R/a =1	R/a =5	R/a =10	R/a =50	Plate
0	ref. [46]	129.9808	94.4973	71.8861	71.0394	70.7660	70.7546
	present $\epsilon_{zz} = 0$	133.6037	95.5849	73.1640	72.3304	72.0614	72.0502
	present $\epsilon_{zz} \neq 0$	134.5056	96.0131	73.6436	72.8141	72.5465	72.5353
0.2	ref. [46]	119.6109	87.3930	68.1152	67.3320	67.0801	67.0698
	present $\epsilon_{zz} = 0$	121.8612	87.8148	66.6620	65.8808	65.6371	65.6299
	present $\epsilon_{zz} \neq 0$	122.7375	88.1659	67.1004	66.3235	66.0814	66.0743
0.5	ref. [46]	108.1546	79.5689	63.1896	62.4687	62.2380	62.2291
	present $\epsilon_{zz} = 0$	110.2017	80.0146	60.2477	59.5215	59.3022	59.2985
	present $\epsilon_{zz} \neq 0$	111.0739	80.3049	60.6568	59.9353	59.7178	59.7142
1	ref. [46]	96.0666	71.2453	56.5546	55.8911	55.6799	55.6722
	present $\epsilon_{zz} = 0$	97.9069	71.6716	53.5430	52.8800	52.6864	52.6856
	present $\epsilon_{zz} \neq 0$	98.7955	71.9167	53.9340	53.2759	53.0841	53.0835
2	ref. [46]	84.4431	62.9748	36.2487	35.6633	35.4745	35.4669
	present $\epsilon_{zz} = 0$	86.3088	63.4398	47.5205	46.9447	46.7820	46.7835
	present $\epsilon_{zz} \neq 0$	87.2271	63.6675	47.9060	47.3343	47.1726	47.1741
10	ref. [46]	69.8224	51.3803	33.6611	33.1474	32.9812	32.9743
	present $\epsilon_{zz} = 0$	71.7634	52.0900	40.8099	40.4145	40.3028	40.3037
	present $\epsilon_{zz} \neq 0$	72.3922	52.2780	41.0985	40.7046	40.5923	40.5929
∞	ref. [46]	61.0568	44.2962	32.4802	32.0976	31.9741	31.9689
	present $\epsilon_{zz} = 0$	60.3660	43.1880	33.0576	32.6810	32.5594	32.5543
	present $\epsilon_{zz} \neq 0$	60.7735	43.3815	33.2743	32.8995	32.7786	32.7735

Table 4
Fundamental frequencies of CCCC square FG cylindrical shell panels composed of aluminum and alumina, $a/h = 10$, for various R/a and p.

4.4 Simply supported functionally graded spherical shell panel

This example considers the free vibration of simply supported FG spherical shell panels.

The fundamental frequency of a square simply supported FG spherical shell panel composed of aluminum (54) and alumina (55), with side-to-thickness ratio $a/h = 10$, are presented in table 7 considering various side-to-radius ratios a/R as well power law exponents p.

p	source	R/a =0.5	R/a =1	R/a =5	R/a =10	R/a =50	Plate
0	ref. [46]	68.8645	51.5216	42.2543	41.9080	41.7963	41.7917
	present $\epsilon_{zz} = 0$	70.1594	52.1938	42.6701	42.3153	42.2008	42.1961
	present $\epsilon_{zz} \neq 0$	69.9872	52.1101	42.7172	42.3684	42.2560	42.2513
0.2	ref. [46]	64.4001	47.5968	40.1621	39.8472	39.7465	39.7426
	present $\epsilon_{zz} = 0$	65.3889	47.9338	38.7168	38.3840	38.2842	38.2827
	present $\epsilon_{zz} \neq 0$	65.2100	47.8590	38.7646	38.4368	38.3384	38.3368
0.5	ref. [46]	59.4396	43.3019	37.2870	36.9995	36.9088	36.9057
	present $\epsilon_{zz} = 0$	60.4255	43.6883	34.8768	34.5672	34.4809	34.4820
	present $\epsilon_{zz} \neq 0$	60.2422	43.6239	34.9273	34.6219	34.5365	34.5376
1	ref. [46]	53.9296	38.7715	33.2268	32.9585	32.8750	32.8726
	present $\epsilon_{zz} = 0$	54.8909	39.1753	30.9306	30.6485	30.5759	30.5792
	present $\epsilon_{zz} \neq 0$	54.7074	39.1246	30.9865	30.7077	30.6355	30.6386
2	ref. [46]	47.8259	34.3338	27.4449	27.1789	27.0961	27.0937
	present $\epsilon_{zz} = 0$	48.7807	34.7654	27.5362	27.2979	27.2423	27.2472
	present $\epsilon_{zz} \neq 0$	48.6005	34.7289	27.5977	27.3616	27.3055	27.3102
10	ref. [46]	37.2593	28.2757	19.3892	19.1562	19.0809	19.0778
	present $\epsilon_{zz} = 0$	38.2792	28.8072	24.2472	24.1063	24.0762	24.0802
	present $\epsilon_{zz} \neq 0$	38.1172	28.7611	24.2839	24.1444	24.1125	24.1171
∞	ref. [46]	31.9866	24.1988	19.0917	18.9352	18.8848	18.8827
	present $\epsilon_{zz} = 0$	31.7000	23.5827	19.2796	19.1193	19.0675	19.0654
	present $\epsilon_{zz} \neq 0$	31.6222	23.5448	19.3008	19.1433	19.0924	19.0903

Table 5
Fundamental frequencies of SSSS square FG cylindrical shell panels composed of aluminum and alumina, $a/h = 10$, for various R/a and p.

4.5 Discussion

All results presented in tables 2 to 7 are in excellent agreement with references considered. Exceptions are $p = 10$ and $R/a = 5, 10, 50$ for the SSSS panels, and $p = 2, 10$ and $R/a = 5, 10, 50$ for the CCCC panels. The authors did not find any explanation for these exceptions.

A detailed analysis of previous tables lead us to the following conclusions:

- **Boundary conditions:** Clamped FG shell panels present higher frequency

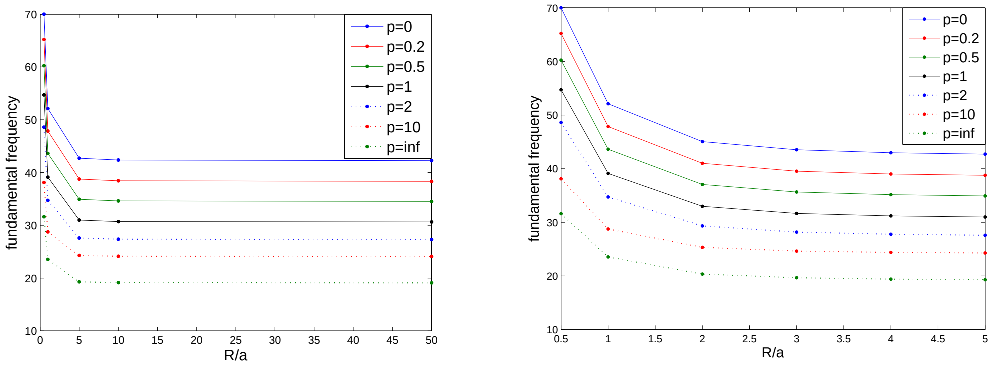

Fig. 4. Fundamental frequency as a function of the radius-to-length ratio for several p.

values than simply supported ones.

- **Geometry:** Lower radii of curvature values present higher frequency values, i. e., the fundamental frequency decreases as the ratio R/a increases.
- **Material properties:** The fundamental frequency of FG shell panels decreases as the exponent p in power-law increases.

Another conclusion from all tables, as easily seen in figure 4, is that the fundamental frequency decreases as the radius of curvature increases. The fall-off is faster for smaller values of R (R/a) and then shows fast convergence.

The effect of $\epsilon_{zz} \neq 0$ shows significance in thicker shells (see table 2) and seems independent of the radius of curvature (see tables 4 to 7).

5 Concluding remarks

For the first time, Carrera's Unified Formulation was combined with the radial basis functions collocation technique for the free vibration analysis of functionally graded shells. A higher-order shear deformation theory that allows extensibility in the thickness direction was implemented and the effect of $\epsilon_{zz} \neq 0$ was studied.

Numerical results were compared with other sources and the present approach demonstrated to be successful in the free vibration analysis of functionally graded shells and easy to implement.

p	source	R/a =0.5	R/a =1	R/a =5	R/a =10	R/a =50	Plate
0	ref. [46]	173.9595	120.9210	73.5550	71.4659	70.7832	70.7546
	present $\epsilon_{zz} = 0$	176.8125	122.0934	74.8207	72.7536	72.0784	72.0502
	present $\epsilon_{zz} \neq 0$	176.8356	122.3533	75.2810	73.2322	72.5633	72.5353
0.2	ref. [46]	161.3704	112.2017	69.6597	67.7257	67.0956	67.0698
	present $\epsilon_{zz} = 0$	163.0852	112.7143	68.2142	66.2686	65.6498	65.6299
	present $\epsilon_{zz} \neq 0$	163.0460	112.8132	68.6329	66.7063	66.0938	66.0743
0.5	ref. [46]	147.4598	102.5983	64.6114	62.8299	62.2519	62.2291
	present $\epsilon_{zz} = 0$	149.0931	103.1804	61.6902	59.8745	59.3112	59.2985
	present $\epsilon_{zz} \neq 0$	149.0095	103.1490	62.0789	60.2831	59.7265	59.7142
1	ref. [46]	132.3396	92.2147	57.8619	56.2222	55.6923	55.6722
	present $\epsilon_{zz} = 0$	133.8751	92.8282	54.8597	53.1956	52.6921	52.6856
	present $\epsilon_{zz} \neq 0$	133.7710	92.6962	55.2302	53.5864	53.0895	53.0835
2	ref. [46]	116.4386	81.3963	37.3914	35.9568	35.4861	35.4669
	present $\epsilon_{zz} = 0$	118.0167	82.0948	48.6656	47.2135	46.7849	46.7835
	present $\epsilon_{zz} \neq 0$	117.9317	81.9179	49.0328	47.5990	47.1754	47.1741
10	ref. [46]	92.1387	64.8773	34.6658	33.4057	32.9916	32.9743
	present $\epsilon_{zz} = 0$	93.9111	65.8103	41.6016	40.5998	40.3049	40.3037
	present $\epsilon_{zz} \neq 0$	93.8398	65.7018	41.8796	40.8883	40.5946	40.5929
∞	ref. [46]	80.7722	56.2999	33.2343	32.2904	31.9819	31.9689
	present $\epsilon_{zz} = 0$	79.8889	55.1653	33.8061	32.8722	32.5671	32.5543
	present $\epsilon_{zz} \neq 0$	79.8994	55.2827	34.0141	33.0884	32.7862	32.7735

Table 6
Fundamental frequencies of CCCC square FG spherical shell panels composed of aluminum and alumina, $a/h = 10$, for various R/a and p.

6 Acknowledgement

The first author is grateful for the grant SFRH/BD/45554/2008 assured by FCT.

p	source	R/a =0.5	R/a =1	R/a =5	R/a =10	R/a =50	Plate
0	ref. [46]	124.1581	78.2306	44.0073	42.3579	41.8145	41.7917
	present $\epsilon_{zz} = 0$	126.2994	79.2626	44.4455	42.7709	42.2192	42.1961
	present $\epsilon_{zz} \neq 0$	126.0882	79.0008	44.4697	42.8180	42.2741	42.2513
0.2	ref. [46]	115.7499	72.6343	41.7782	40.2608	39.7629	39.7426
	present $\epsilon_{zz} = 0$	117.3053	73.2663	40.3936	38.8074	38.2988	38.2827
	present $\epsilon_{zz} \neq 0$	117.0197	73.0034	40.4211	38.8551	38.3528	38.3368
0.5	ref. [46]	106.5014	66.5025	38.7731	37.3785	36.9234	36.9057
	present $\epsilon_{zz} = 0$	108.0044	67.1623	36.4453	34.9574	34.4922	34.4820
	present $\epsilon_{zz} \neq 0$	107.6572	66.9033	36.4782	35.0080	34.5478	34.5376
1	ref. [46]	96.2587	59.8521	34.6004	33.3080	32.8881	32.8726
	present $\epsilon_{zz} = 0$	97.6938	60.5121	32.3691	31.0012	30.5840	30.5792
	present $\epsilon_{zz} \neq 0$	97.2968	60.2636	32.4101	31.0572	30.6437	30.6386
2	ref. [46]	84.8206	52.7875	28.7459	27.5110	27.1085	27.0937
	present $\epsilon_{zz} = 0$	86.2288	53.4659	28.7833	27.5984	27.2474	27.2472
	present $\epsilon_{zz} \neq 0$	85.8028	53.2311	28.8329	27.6602	27.3109	27.3102
10	ref. [46]	65.2296	41.6702	20.4691	19.4357	19.0922	19.0778
	present $\epsilon_{zz} = 0$	66.7088	42.4365	25.0772	24.3034	24.0791	24.0802
	present $\epsilon_{zz} \neq 0$	66.3594	42.2155	25.1038	24.3401	24.1168	24.1171
∞	ref. [46]	57.2005	36.2904	19.8838	19.1385	18.8930	18.8827
	present $\epsilon_{zz} = 0$	57.0657	35.8131	20.0818	19.3251	19.0759	19.0654
	present $\epsilon_{zz} \neq 0$	56.9702	35.6948	20.0927	19.3464	19.1006	19.0903

Table 7
Fundamental frequencies of SSSS square FG spherical shell panels composed of aluminum and alumina, $a/h = 10$, for various R/a and p.

References

[1] M.B. Bever and P.E. Duwez. Gradients in composite materials. *Materials Science and Engineering*, 10(0):1 – 8, 1972.

[2] Y. Miyamoto, W.A. Kaysser, B.H. Rabin, A. Kawasaki, and R.G. Ford. *Functionally Graded Materials: Design, Processing and Applications.* Kluwer Academic Publishers, 1999.

[3] F.J. Ferrante and L.L. Graham-Brady. Stochastic simulation of non-gaussian/non-stationary properties in a functionally graded plate. *Computer*

Methods in Applied Mechanics and Engineering, 194(12-16):1675 – 1692, 2005.

[4] H.M Yin, L.Z Sun, and G.H Paulino. Micromechanics-based elastic model for functionally graded materials with particle interactions. *Acta Materialia*, 52(12):3535 – 3543, 2004.

[5] Zheng Zhong and Ertao Shang. Closed-form solutions of three-dimensional functionally graded plates. *Mechanics of Advanced Materials and Structures*, 15(5):355–363, 2008.

[6] T. K. Nguyen, K. Sab, and G. Bonnet. Shear correction factors for functionally graded plates. *Mechanics of Advanced Materials and Structures*, 14(8):567–575, 2007.

[7] Victor Birman and Larry W. Byrd. Modeling and analysis of functionally graded materials and structures. *Applied Mechanics Reviews*, 60(5):195–216, 2007.

[8] M. Koizumi. Fgm activities in japan. *Composites Part B: Engineering*, 28(1-2):1 – 4, 1997. Use of Composites Multi-Phased and Functionally Graded Materials.

[9] E. Carrera. Theories and finite elements for multilayered plates and shells: a unified compact formulation with numerical assessment and benchmarking. *Archives of Computational Methods in Engineering*, 10:215–296, 2003.

[10] D. Chapelle and K.-J. Bathe. *The finite element analysis of shells.-Fundamentals*. Springer, Berlin, 2003.

[11] W. Flügge. *Stresses in shells*. 2nd edn. Springer, Berlin, 1960.

[12] A. Scordelis and K. S. Lo. Computer analysis in cylindrical shells. *Journal of American Concrete Institute*, 61:561–593, 1964.

[13] J. N. Reddy. Bending of laminated anisotropic shells by a shear deformable finite element. *Fibre Science and Technology*, 17:9–24, 1982.

[14] E. J. Kansa. Multiquadrics- a scattered data approximation scheme with applications to computational fluid dynamics. i: Surface approximations and partial derivative estimates. *Computers and Mathematics with Applications*, 19(8/9):127–145, 1990.

[15] Y. C. Hon, M. W. Lu, W. M. Xue, and Y. M. Zhu. Multiquadric method for the numerical solution of byphasic mixture model. *Applied Mathematics and Computation*, 88:153–175, 1997.

[16] Y. C. Hon, K. F. Cheung, X. Z. Mao, and E. J. Kansa. A multiquadric solution for the shallow water equation. *ASCE Journal of Hydraulic Engineering*, 125(5):524–533, 1999.

[17] J. G. Wang, G. R. Liu, and P. Lin. Numerical analysis of biot's consolidation process by radial point interpolation method. *International Journal of Solids and Structures*, 39(6):1557–1573, 2002.

[18] G. R. Liu and Y. T. Gu. A local radial point interpolation method (lrpim) for free vibration analyses of 2-d solids. *Journal of Sound and Vibration*, 246(1):29–46, 2001.

[19] G. R. Liu and J. G. Wang. A point interpolation meshless method based on radial basis functions. *International Journal for Numerical Methods in Engineering*, 54:1623–1648, 2002.

[20] J. G. Wang and G. R. Liu. On the optimal shape parameters of radial basis functions used for 2-d meshless methods. *Computer Methods in Applied Mechanics and Engineering*, 191:2611–2630, 2002.

[21] X. L. Chen, G. R. Liu, and S. P. Lim. An element free galerkin method for the free vibration analysis of composite laminates of complicated shape. *Composite Structures*, 59:279–289, 2003.

[22] K. Y. Dai, G. R. Liu, S. P. Lim, and X. L. Chen. An element free galerkin method for static and free vibration analysis of shear-deformable laminated composite plates. *Journal of Sound and Vibration*, 269:633–652, 2004.

[23] G. R. Liu and X. L. Chen. Buckling of symmetrically laminated composite plates using the element-free galerkin method. *International Journal of Structural Stability and Dynamics*, 2:281–294, 2002.

[24] K. M. Liew, X. L. Chen, and J. N. Reddy. Mesh-free radial basis function method for buckling analysis of non-uniformity loaded arbitrarily shaped shear deformable plates. *Computer Methods in Applied Mechanics and Engineering*, 193:205–225, 2004.

[25] Y. Q Huang and Q. S. Li. Bending and buckling analysis of antisymmetric laminates using the moving least square differential quadrature method. *Computer Methods in Applied Mechanics and Engineering*, 193:3471–3492, 2004.

[26] L. Liu, G. R. Liu, and V. C. B. Tan. Element free method for static and free vibration analysis of spatial thin shell structures. *Computer Methods in Applied Mechanics and Engineering*, 191:5923–5942, 2002.

[27] S. Xiang, K. M. Wang, Y. T. Ai, Y. D. Sha, and H. Shi. Analysis of isotropic, sandwich and laminated plates by a meshless method and various shear deformation theories. *Composite Structures*, 91(1):31–37, 2009.

[28] S. Xiang, H. Shi, K. M. Wang, Y. T. Ai, and Y. D. Sha. Thin plate spline radial basis functions for vibration analysis of clamped laminated composite plates. *European Journal of Mechanics A/Solids*, 29:844–850, 2010.

[29] Ferreira A. J. A. Roque, C. M. C. and R. M. N. Jorge. Analysis of composite and sandwich plate by trigonometric layer-wise deformation theory and radial basis function. *J. Sandwich Struct. Mater.*, 8:497–515, 2006.

[30] A. J. M. Ferreira. A formulation of the multiquadric radial basis function method for the analysis of laminated composite plates. *Composite Structures*, 59:385–392, 2003.

[31] A. J. M. Ferreira. Thick composite beam analysis using a global meshless approximation based on radial basis functions. *Mechanics of Advanced Materials and Structures*, 10:271–284, 2003.

[32] A. J. M. Ferreira, C. M. C. Roque, and P. A. L. S. Martins. Analysis of composite plates using higher-order shear deformation theory and a finite point formulation based on the multiquadric radial basis function method. *Composites: Part B*, 34:627–636, 2003.

[33] A.J.M. Ferreira, C.M.C. Roque, E. Carrera, M. Cinefra, and O. Polit. Radial basis functions collocation and a unified formulation for bending, vibration and buckling analysis of laminated plates, according to a variation of murakamiâĂŹs zig-zag theory. *European Journal of Mechanics - A/Solids*, 30(4):559 – 570, 2011.

[34] J.D. Rodrigues, C.M.C. Roque, A.J.M. Ferreira, E. Carrera, and M. Cinefra. Radial basis functions-finite differences collocation and a unified formulation for bending, vibration and buckling analysis of laminated plates, according to murakami's zig-zag theory. *Composite Structures*, 93(7):1613 – 1620, 2011.

[35] A.J.M. Ferreira, C.M.C. Roque, E. Carrera, and M. Cinefra. Analysis of thick isotropic and cross-ply laminated plates by radial basis functions and a unified formulation. *Journal of Sound and Vibration*, 330(4):771 – 787, 2011.

[36] A. J.M. Ferreira, C. M.C. Roque, E. Carrera, M. Cinefra, and O. Polit. Two higher order zig-zag theories for the accurate analysis of bending, vibration and buckling response of laminated plates by radial basis functions collocation and a unified formulation. *Journal of Composite Materials*, 2011.

[37] A. Ferreira, E. Carrera, M. Cinefra, and C. Roque. Analysis of laminated doubly-curved shells by a layerwise theory and radial basis functions collocation, accounting for through-the-thickness deformations. *Computational Mechanics*, 48:13–25, 2011. 10.1007/s00466-011-0579-4.

[38] A.J.M. Ferreira, E. Carrera, M. Cinefra, C.M.C. Roque, and O. Polit. Analysis of laminated shells by a sinusoidal shear deformation theory and radial basis functions collocation, accounting for through-the-thickness deformations. *Composites Part B: Engineering*, 42(5):1276 – 1284, 2011.

[39] A.M.A. Neves, A.J.M. Ferreira, E. Carrera, C.M.C. Roque, M. Cinefra, R.M.N. Jorge, and C.M.M. Soares. Bending of fgm plates by a sinusoidal plate formulation and collocation with radial basis functions. *Mechanics Research Communications*, 38(5):368 – 371, 2011.

[40] A.M.A. Neves, A.J.M. Ferreira, E. Carrera, C.M.C. Roque, M. Cinefra, R. M.N. Jorge, and C.M.M. Soares. A quasi-3d sinusoidal shear deformation theory for the static and free vibration analysis of functionally graded plates. *Composites Part B*, In Press, Accepted Manuscript:–, 2011.

[41] E. Carrera. Developments, ideas, and evaluations based upon reissner's mixed variational theorem in the modelling of multilayered plates and shells. *Applied Mechanics Reviews*, 54:301–329, 2001.

[42] E. Carrera. On the use of murakami's zig-zag function in the modeling of layered plates and shells. *Compos. Struct.*, 82:541–554, 2004.

[43] E. Carrera and S.Brischetto. Analysis of thickness locking in classical, refined and mixed theories for layered shells. *Composite Structures*, 85:83–90, 2008.

[44] M. Soave M. Cinefra, S. Belouettar and E. Carrera. Variable kinematic models applied to free-vibration analysis of functionally graded material shells. *European Journal of Mechanics A/Solids*, 29:1078–1087, 2010.

[45] B. Kröplin M. D'Ottavio, D. Ballhause and E. Carrera. Closed-form solutions for the free-vibration problem of multilayered piezoelectric shells. *Computers and Structures*, 84:1506–1518, 2006.

[46] S. Pradyumna and J.N. Bandyopadhyay. Free vibration analysis of functionally graded curved panels using a higher-order finite element formulation. *Journal of Sound and Vibration*, 318(1-2):176 – 192, 2008.

[47] A. J. M. Ferreira and G. E. Fasshauer. Computation of natural frequencies of shear deformable beams and plates by a rbf-pseudospectral method. *Computer Methods in Applied Mechanics and Engineering*, 196:134–146, 2006.

[48] J. Yang and Hui-Shen Shen. Free vibration and parametric resonance of shear deformable functionally graded cylindrical panels. *Journal of Sound and Vibration*, 261(5):871 – 893, 2003.